ACS Catalysis

Research Article

pubs.acs.org/acscatalysis

Proton-Conducting Perovskites as Supports for Cr Catalysts in Short Contact Time Ethane Dehydrogenation

Hyun Ho Shin and Steven McIntosh*

Department of Chemical Engineering, Lehigh University, Bethlehem, Pennsylvania 18015, United States

Supporting Information

ABSTRACT: Proton-conducting oxides, $BaZrO_3$ (BZ) and $BaCeO_3$ (BC), were investigated as potential support materials for Cr catalyst (0.2−0.6 wt % Cr, Cr/BZ or BC) in ethane dehydrogenation at short contact times. The catalytic activity, selectivity in ethane dehydrogenation, and carbon formation were determined. A higher ethylene formation rate was obtained on Cr/BZ in comparison to Cr/BC: 1.4×10^{-7} and 6.2×10^{-8} mol/m^2 s at 575 °C at 1 min on stream for 1 g of 0.2 Cr/BZ and 0.2 Cr/BC, respectively. The selectivity was maintained above 94% over all samples in the temperature range 475−575 °C. The catalytic activity toward ethane dehydrogenation was more than 1 order of magnitude higher for the proton-conducting supports when in comparison to a Cr/γ-Al_2O_3 catalyst with similar surface Cr coverage. X-ray photoelectron spectroscopy (XPS) revealed an initially higher concentration of Cr^{6+} on Cr/BC in comparison to Cr/BZ, corresponding to a plateau of relatively high activity at short times on stream. This plateau is attributed to oxidation of surface carbon species as they form via reduction of Cr^{6+} to Cr^{3+}. All of the catalysts show deactivation through carbon deposition; however, the higher activity of proton-conducting supports may enable commercial operation at reduced temperature and thus reduced coke formation. A decreased residence time led to a significant increase of ethylene concentration at the reactor outlet with an associated decrease in carbon formation. Addition of H_2 to the reactant feed further suppressed carbon formation but resulted in a significant decrease in ethylene formation rate.

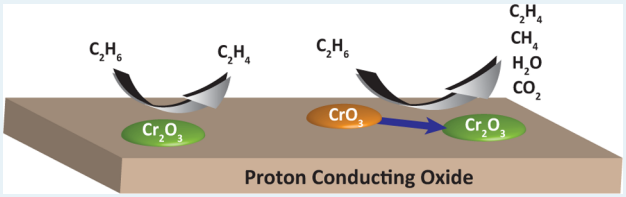

KEYWORDS: *ethane, dehydrogenation, chromium, proton conducting perovskite, carbon deposition*

1. INTRODUCTION

Alkane dehydrogenation, to produce light olefins from C_2−C_4 saturated hydrocarbon feedstock, is a key reaction in the chemical industry, especially as we seek to fully utilize natural gas resources from fracking. The most commonly utilized process for ethylene production is energy-intensive noncatalytic steam cracking at high temperature.[1−3] In the last few decades, catalytic oxidative ethane dehydrogenation has received increasing attention, as it operates at reduced temperature and can potentially provide higher ethylene yields;[4,5] however, the oxidizing atmosphere leads to a number of issues such as significant loss of produced hydrogen as water and undesirable complete oxidation to CO_2.[3]

Nonoxidative alkane dehydrogenation over supported metal catalysts has been investigated as an alternative. Finely dispersed platinum and chromium supported on high-surface-area oxides are the most commonly studied catalysts.[1,6] Among those, supported Cr_2O_3 over Al_2O_3 catalysts are widely used as commercial catalysts on account of their outstanding properties for alkane dehydrogenation.[7] The support material plays an important role in determining reaction selectivity in these systems, with unsupported catalysts yielding low ethylene selectivity and rapid deactivation via carbon deposition.[8,9] Carbon deposition is common on these catalysts, requiring the reactor to be cycled for regenerations: for example, in the CATOFIN process. A reduction in operating temperature provided by a more active catalyst would lead to longer on-stream times.

In this study, our primary focus is the possible use of a proton-conducting ceramic as a support material for these reactions. The use of a proton-conducting support can potentially open up a new reaction pathway. In the case of proton-conducting oxide, the protonic formation reaction may be described with the incorporation of water on a vacant oxygen site:

$$H_2O(g) + V_o^{\bullet\bullet} + O_o^x \leftrightarrow OH_o^{\bullet} \quad (1)$$

or as incorporation of H_2

$$H_2(g) + 2O_o^x \leftrightarrow 2OH_o^{\bullet} + 2e^- \quad (2)$$

The incorporated proton may be considered as hydroxide ions on an oxide ion sites, $OH_o^{\bullet}$ in Kröger−Vink notation. This incorporation mechanism is analogous to the well-studied Mars−van Krevelen mechanism for oxygen in oxidation catalysis. Developing catalytic systems that can utilize this pathway may dramatically enhance the activity of supported heterogeneous catalyst for reactions involving hydrogen, particularly when hydrogen spillover to the support is expected

Received: September 2, 2014
Revised: November 11, 2014
Published: November 13, 2014

 © 2014 American Chemical Society

to play an important mechanistic role. We have previously demonstrated that hydrogen spillover from metals to the support is the most likely mechanism of proton incorporation in these materials.[10,11]

In addition to potentially opening new reaction pathways through proton incorporation in the support material,[12] the use of a proton-conducting support opens the possibility of creating electrochemical reactor systems for the cogeneration of olefins and electricity.[13−17] Hydrogen obtained from alkane dehydrogenation would be utilized as fuel for the proton-conducting solid oxide fuel cell with the product olefin generated at the cell anode. For example, Fu et al.[14] identified the ethane-fueled proton-conducting solid oxide fuel cell with Cr_2O_3 as a bulk anode catalyst, exhibiting cogeneration with 17.1% ethylene yields and 85 mW/cm^2 at 700 °C with stable performance for 48 h. Heterogeneous catalysis has an important role to play in aiding the development of selective catalysts for these high-temperature electrochemical systems.[15,18,19]

Despite the potential industrial importance of nonoxidative alkane dehydrogenation, there is only limited information regarding supported chromium catalysts in the literature. It is generally accepted that the surface chromium oxidation state is important in determining both activity and selectivity, but there is some debate concerning the nature of the primary active site: between Cr^{3+}, regarded as dominant in the most recent studies, and Cr^{2+}.[8,20] The influence of the support material on chromium oxidation state is also unclear. A significant support effect was clearly observed in isobutane dehydrogenation,[21,22] while no significant effect was observed between Al_2O_3 and SiO_2 in ethane dehydrogenation.[8]

There are a number of additional intriguing observations previously reported for these reacting systems. For example, a number of groups have observed a delayed onset in maximum olefin production rates upon starting the reactor. Nijhuis et al.[23] suggested that this delayed maximum in product yields is associated with initial reconsumption of product alkene by further reduction of chromium from Cr^{6+} to Cr^{3+}. In contrast, Olsbye et al.,[24] who observed maximum ethylene yields after about 10 min in on-stream for ethane dehydrogenation over Cr/Al_2O_3, attributed this to the formation of an active hydrocarbon intermediate on the surface. Catalyst deactivation via carbon formation is a significant issue for dry alkane dehydrogenation on the industrial scale, but this report suggests that a small amount of carbon deposition may be beneficial. In either case, secondary reactions of product olefins on the catalyst both decrease product yield and lead to excessive carbon deposition. Thus, maximizing the olefin yield is favored by short contact time in the reactor.

In this work, we study barium cerates and zirconates, which are among the most promising proton-conducting oxides,[25] as supports for Cr catalysts in ethane dehydrogenation. In addition to measuring reaction rates and selectivity, the influence of support material on Cr oxidation state was determined. The reaction was conducted with different residence times to elucidate the carbon formation reaction mechanism from product ethylene over supported Cr catalyst on proton-conducting oxides. The influence of water and H_2 on carbon formation during ethane dehydrogenation is discussed.

2. EXPERIMENTAL SECTION

2.1. Sample Preparation. $BaCeO_3$ (BC) and $BaZrO_3$ (BZ) powders were synthesized utilizing a modified Pechini method.[10,26] Aqueous solutions of Ba, Ce, and Zr (>99% pure, Alfa Aesar, Ward Hill, MA, USA) nitrate salts were prepared, and the metal concentrations were determined by redox titration.[27] The solutions were mixed, in the stoichiometric ratio to fabricate the desired composition, with the chelating agent EDTA (99%, Alfa Aesar, Ward Hill, MA) and citric acid monohydrate (99.0−102.0%, Alfa Aesar). The pH was adjusted to >8.5 by addition of ammonium hydroxide (14.8 N, Fisher Scientific), and excess water was evaporated. The resulting homogeneous gel was combusted in an oven at 300 °C and the resulting powder sintered for 4 h at 1100 and 1300 °C for BC and BZ, respectively. Cr catalyst supported on the synthesized pure oxide (0.2−0.6 wt % Cr, denoted 0.2−0.6 Cr/BC or Cr/BZ in the following) were fabricated using a standard incipient wetness procedure.[10,28] γ-Al_2O_3 (>99% pure, Alfa Aesar, Ward Hill, MA, USA) was employed for Cr catalyst supported on Al_2O_3. Aqueous solutions of Cr (>93% pure, Alfa Aesar, Ward Hill, MA, USA) were prepared and the concentrations determined by redox titration. A 10 wt % amount of Cr was deposited on the Al_2O_3 support to maintain approximately constant Cr content per unit surface area of catalyst support between the higher surface area Al_2O_3 and lower surface area perovskite support materials.

2.2. Catalyst Characterization. The synthesized materials were characterized by powder X-ray diffraction with Cu Kα radiation and fixed slit width (MiniFlex (II), Rigaku, The Woodlands, TX, USA). Diffraction patterns were recorded in the 2θ range of 20−70° with a step size of 0.02° and a counting time of 0.2 min/deg. The BET surface area (ASAP2020, micrometrics, Norcross, GA, USA) was measured using N_2 and krypton gas as the absorbent after samples were degassed at 300 °C for 10 h. X-ray photoelectron spectra (XPS) measurements were conducted to investigate the oxidation state of supported Cr catalyst. Prior to XPS measurement, samples were oxidized to remove surface contaminants at 800 °C for 1 h in a flow of 50 mL/min 19.5−23.5 vol % O_2/N_2 (GTS-Welco, Allentown, PA, USA), and then reduced at 600 °C under flowing 5 vol % H_2/Ar (UHP gases, <1 ppm of O_2, GTS-Welco, Allentown, PA, USA) for 1 h. The samples were pressed onto conductive tape with moderate pressure and transferred to a sample holder. The spectra were obtained on a Scienta ESCA-300 with monochromatic X-ray (beam spot, 5 mm × 1 mm) generated by an Al Kα source (E = 1486 eV).

2.3. Catalyst Testing. Ethane dehydrogenation was conducted with the sieved powder (106−150 μm) as a fixed bed in a continuous flow quartz tube reactor. The size of the reactor was varied according to the sample size for different residence times: i.d. 8 and 4 mm in the cases of 1 g and below 0.2 g, respectively, with the same length of 300 mm. Quartz glass wool was used to hold the powder sample in the center of the reactor. Gas flows were regulated by mass flow controllers (Brooks, 4850 series, Exton, PA, USA). Prior to measurement the samples were heated to 800 °C at a rate of 10 °C/min in a flow of 100 mL/min dry air with <0.5 ppm of CO_2 and then held for 1 h at this temperature to remove moisture and contaminants on the surface of the powder sample. The powder sample was cooled to 600 °C under the same flow conditions and subsequently reduced at 600 °C for 1 h under flowing 50 mL/min 5 vol % H_2/N_2. The reactor was flushed with nitrogen and cooled to measurement temperature after this pretreatment, prior to feeding the reactant mixture of 5 vol % ethane/N_2 (UHP gases, <1 ppm of O_2, GTS-Welco, Allentown, PA, USA) at 150 mL/min at measurement temperature. This

dx.doi.org/10.1021/cs501314w | ACS Catal. 2015, 5, 95−103

procedure was repeated with steps of 25 °C between 475 and 575 °C.

The concentrations of reactants and products were analyzed for 2 h at each temperature using an online gas chromatograph (SRI 8610C, CA, USA) with a 10-port sampling valve and a Haysep D columns. A thermal conductivity detector (TCD) was used to measure the concentration of product eluting from the column. The testing process was also repeated for 0.2Cr/BC using a residual gas analyzer (RGA) fitted with a quadropole analyzer and associated Faraday and secondary electron multiplier detectors (Cirrus 2, MKS Instruments UK Ltd.) to qualitatively observe any CO or CO_2 production during the initial few minutes on-stream. To study the influence of residence time, the sample size was varied from 0.1 to 1 g. The effect of hydrogen on ethane dehydrogenation was investigated by addition of hydrogen from 1 to 10 vol % into the ethane flow. Following reaction at each temperature, the carbon deposited on the sample was measured by a temperature-programmed oxidation procedure (TPO) prior to measurement at the next temperature. The tested samples were cooled to room temperature in flowing N_2 prior to TPO. TPO was performed by flowing 100 mL/min 10 vol % O_2 in Ar through the catalyst and ramping the temperature by 10 °C/min from 25 to 800 °C. The CO_2 (m/e 44) concentrations in the reactor effluent were monitored (sampling frequency 1.67 s^{-1}) using a residual gas analyzer (RGA) fitted with a quadrupole analyzer and associated Faraday and secondary electron multiplier detectors (Cirrus 2, MKS Instruments UK Ltd.). The amount of deposited carbon was determined by the amount of generated CO_2 calculated from numerical integration of the CO_2 peak area. The CO_2 peak area was calibrated by using a 100 μL pulse of CO_2. The deactivated powder sample was burned off by an oxidization process at 800 °C in a flow of 100 mL/min dry air with <0.5 ppm of CO_2.

The reaction rate and ethylene yield were calculated assuming a first-order reaction with both being normalized by surface area of loaded powder sample:

$$Y_{C_2H_4}(\%) = \frac{F_{out}[C_2H_4]}{F_{in}[C_2H_6]} \times 100 \quad (1)$$

where F_{in} and F_{out} are the inlet and outlet molar flow rates. The selectivity to C_2H_4 was determined from eq 2.

$$S_{C_2H_4}(\%) = \frac{[C_2H_4]}{([C_2H_6] + 0.5[CH_4])} \times 100 \quad (2)$$

Note that the only secondary gas product was methane. The ethylene formation rate, $R_{C_2H_4}$ (mol of C_2H_4 m^{-2} s^{-1}) of ethane dehydrogenation was evaluated with the ethylene yield measured at 1 min, normalized to the total surface area, S, of the loaded powder sample.

$$R_{C_2H_4} = F_{in}[C_2H_6]\frac{X_{C_2H_4}}{S}$$

3. RESULTS

3.1. Catalyst Characterization. Figure 1 shows the X-ray diffraction patterns of the as-synthesized BC and BZ powders. The patterns for BC and BZ were indexed to an orthorhombic perovskite (space group $Pmcn$)[29−32] and a cubic perovskite structure (space group $Pm\bar{3}m$),[33−35] respectively. Note that BC will transform to a cubic structure at the reaction temperatures

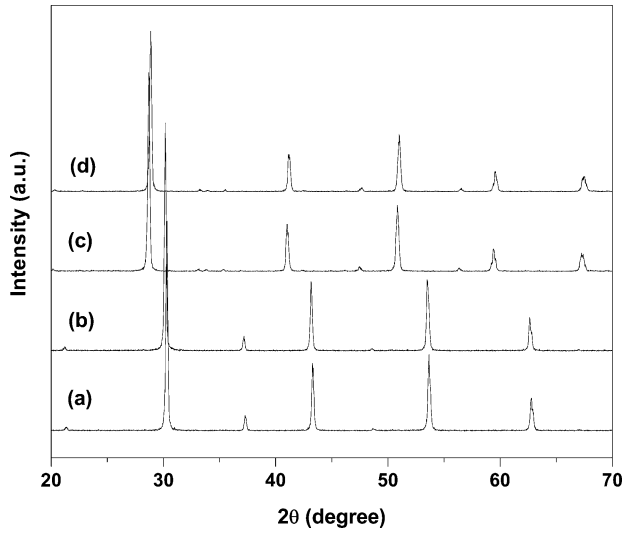

Figure 1. X-ray diffraction patterns of (a) BZ, (b) 0.6 Cr/BZ, (c) BC, and (d) 0.6 Cr/BC.

of interest in this study.[30] XRD analysis could not detect a Cr phase on the supported Cr catalysts due to the low loading. BET surface areas ranged from 1.67 m^2/g for 0.6 Cr/BZ to 3.16 m^2/g for 0.2 Cr/BC (Table 1). These give Cr coverages of 0.19, 0.1, and 0.11 g/m^2 for 10 Cr/Al, 0. 2Cr/BZ, and 0.2 Cr/BC, respectively. The measurement using krypton gas as an absorbent showed 10% lower surface area: 1.89 and 2.20 m^2/g for 0.2 Cr/BZ and 0.4 Cr/BZ.

Table 1. BET Surface Areas

	support						
	Al	BZ			BC		
Cr loading (wt %)	10	0.2	0.4	0.6	0.2	0.4	0.6
surface area (m^2/g)	53.7	2.01	2.48	1.67	3.16	2.4	1.76

3.2. Catalytic Performance of Cr/BZ and Cr/BC. Prior to ethane dehydrogenation with catalyst, the possibility of gas-phase homogeneous dehydrogenation was investigated with a blank reactor, including only quartz wool, in the temperature range 25−750 °C. No ethane conversion was observed below 650 °C; the conversion increased to 3% at 700 °C. Similarly, no C_2H_4 formation was observed over 1 g of pure BC and BZ support at temperatures below 600 °C. The ethane conversion was 0.3% under these conditions and is attributed to a small amount of carbon deposition on the bare support. The low activity over and minimal carbon deposition on the bare support materials indicate that the support materials are inactive for the desired reaction.

Figure 2 shows ethylene yield as a function of time over 1 g of 0.2 Cr/BZ and 0.2 Cr/BC. Note that the ethylene yield reported in the figure is for gas-phase products only and is normalized by the total surface area of the powder sample. The initial ethylene yield, measured at 1 min on-stream, increased with increasing temperature for all catalysts. For example, the yields over 0.2% Cr/$BaZrO_3$ were 0.8, 1.2, 1.6, 2.2, and 2.9% at 475, 500, 525, 550, and 575 °C, respectively. As can be observed for 0.2 Cr/BZ in Figure 2, all of the BZ samples showed rapid deactivation over the 2 h testing period. In

dx.doi.org/10.1021/cs501314w | ACS Catal. 2015, 5, 95−103

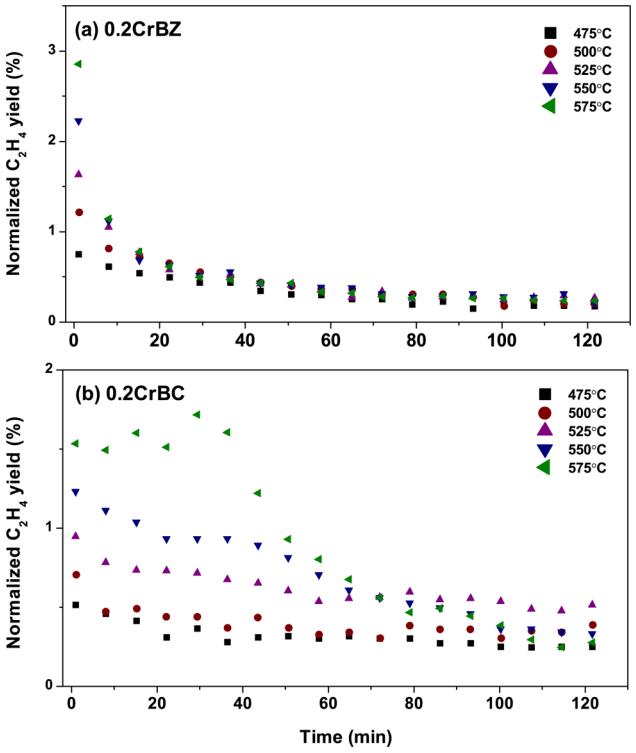

Figure 2. Normalized ethylene yields versus time on-stream over (a) 0.2 Cr/BZ and (b) 0.2 Cr/BC.

contrast, the BC-supported catalysts all showed a more gradual deactivation, particularly as the temperature was increased. This is shown in Figure 2b, where the 0.2Cr/BC sample is relatively stable for the first 40 min.

The C_2H_4 formation rate was calculated from the ethylene yield measured at 1 min on-stream for all of the catalysts (Figure 3). At constant Cr loading, the rates observed for the BZ support were higher than those for BC. In addition, higher Cr loading generally leads to higher formation rate for both supports. The formation rates were 8.3×10^{-8}, 1.0×10^{-7}, and 1.2×10^{-7} mol/(m^2 s) for 0.2, 0.4, and 0.6 Cr/BZ at 525 °C and 4.8×10^{-8}, 6.7×10^{-8}, and 1.0×10^{-7} mol/(m^2 s) for 0.2, 0.4, and 0.6 Cr/BC. It is further observed that the activation energy of supported Cr catalysts on BZ was greater than that on BC.

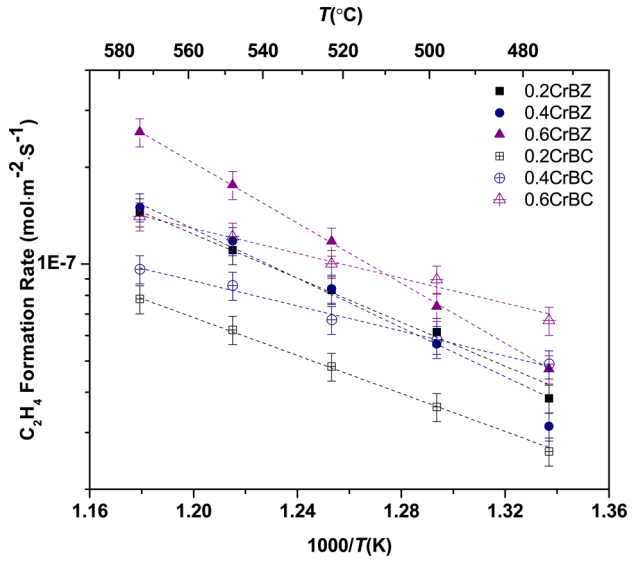

Figure 3. Arrhenius plot of ethylene formation rate over Cr/BZ and Cr/BC at 1 min on-stream.

The gas-phase hydrocarbon product selectivity to C_2H_4 for each catalyst was calculated for the 1 min on-stream data (Figure 4). The only other gas-phase products detected were

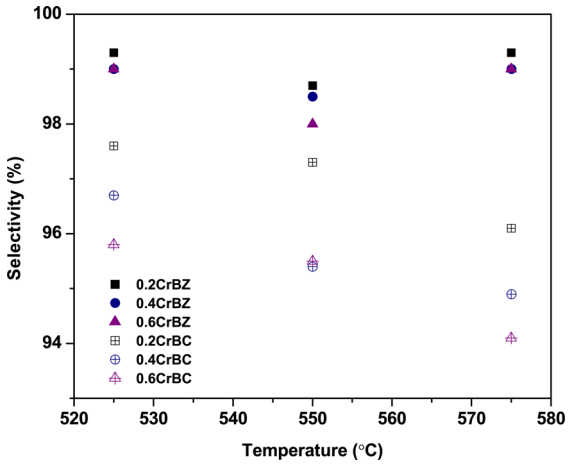

Figure 4. Selectivity to ethylene over Cr/BZ and Cr/BC as a function of temperature at 1 min on-stream.

CH_4 and H_2. The C_2H_4 selectivity of Cr/BZ was maintained above 98%, whereas that of Cr/BC decreased with increasing temperature but was still above 90%. For example, the C_2H_4 selectivities of 0.2 Cr/BZ were 99.3, 98.7, and 99.3% at 525, 550, and 575 °C and those of 0.2 Cr/BC were 97.6, 97.3, and 94.9%, respectively. Note that the C_2H_4 selectivity rose with time on-stream, reaching 100% at 7 and 30 min on-stream for BZ and BC, respectively.

As mentioned previously, the selectivity shown in Figure 4 is for gas-phase products and does not account for carbonaceous deposits. Carbon tolerance is another significant criterion to evaluate the catalysts for potential industrial application. This was evaluated by performing TPO experiments to quantify the amount of carbon deposited; an example of the TPO data is provided in Figure 5a. In all cases, CO_2 evolution was observed as a single peak with a maximum at ∼350 °C. This suggests that the deposited carbon is not graphitic. The calculated amount of carbon deposited on Cr catalysts determined by TPO was normalized by total surface area of the powder sample (Figure 5b). The amount of carbon deposited on all Cr catalysts exponentially increased with increasing temperature; supported Cr catalysts on BC showed significantly larger amounts of carbon deposited in comparison to those on BZ. For example, the amounts of carbon deposited on 0.2, 0.4, and 0.6 Cr/BC were 1.46×10^{-4}, 2.88×10^{-4}, and 3.97×10^{-4} g/m^2 and those for BZ were 1.25×10^{-4}, 1.55×10^{-4}, and 2.28×10^{-4} g/m^2. The normalized conversion of total ethane feed to coke formation was calculated; the normalized conversions for 0.2, 0.4, and 0.6 Cr/BZ were 1.42×10^{-2}, 1.76×10^{-2}, and 2.60×10^{-2} % and those for 0.2, 0.4, and 0.6 Cr/BC were 1.67×10^{-2}, 3.28×10^{-2}, and 4.53×10^{-2} %. It should be noted that the deactivation times between CrBZ and CrBZ were quite different; thus, direct comparison was not available. Note that a small amount of CO (m/e 28) was detected in the TPO experiment; this was expected from fragmentation of CO_2 in the mass spectrometry.

dx.doi.org/10.1021/cs501314w | ACS Catal. 2015, 5, 95−103

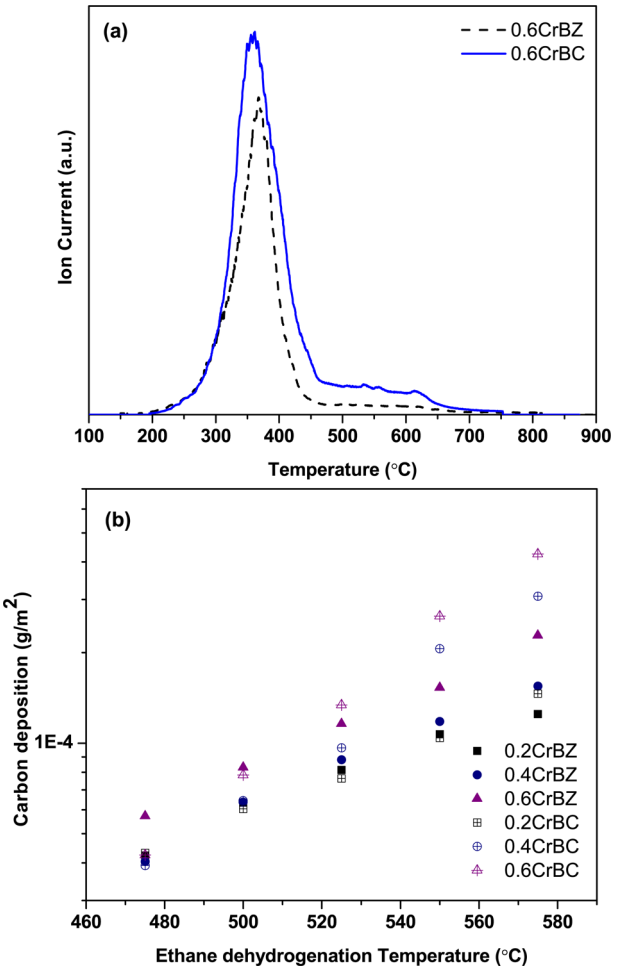

Figure 5. (a) Temperature-programmed oxidation (TPO) data showing CO_2 evolution (m/e 44) of carbon deposited during ethane dehydrogenation over 0.6 Cr/BZ and 0.6 Cr/BC at 575 °C. (b) Amount of carbon deposited (g/m^2) over Cr/BZ and Cr/BC as a function of temperature.

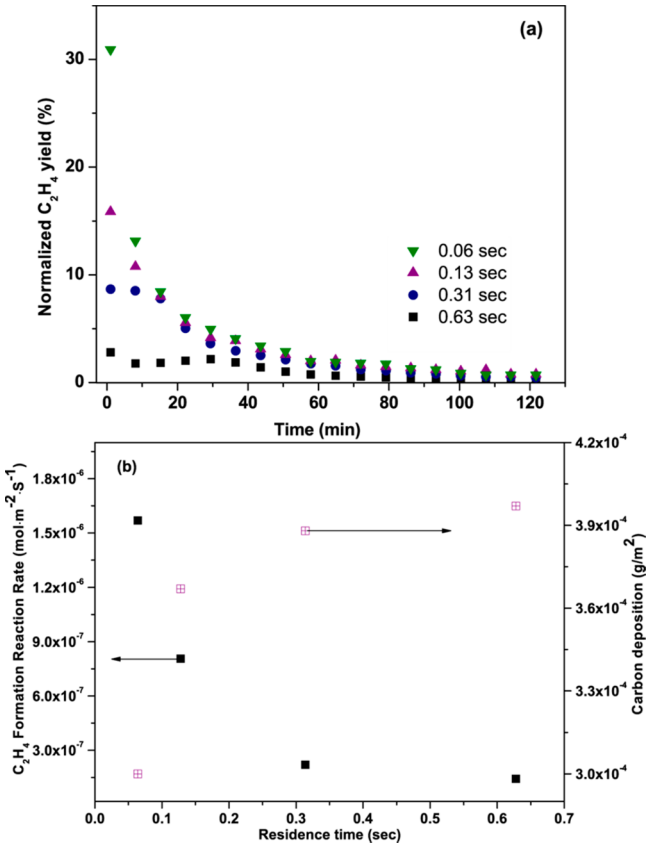

Figure 6. (a) Normalized ethylene yields versus time on stream over 0.6 CrBC at different residence times: 0.06, 0.13, 0.31, and 0.63 s at 575 °C. (b) Ethylene formation rate, selectivity to ethylene, and the amount of carbon deposited as a function of residence time at 575 °C.

3.3. Influence of Residence Time. Figure 6 shows the influence of residence time on ethane dehydrogenation with 0.6 Cr/BC at 575 °C. The initial measurement was conducted at 1 min regardless of the variation of residence time. Figure 6a shows that the C_2H_4 formation at 1 min increased with decreasing residence time. The ethylene yields at 1 min were 2.8, 8.6, 10.2, and 30.9% for residence times of 0.63, 0.31, 0.13, and 0.06 s, respectively. In contrast, no significant difference in yield was observed between different residence times after 60 min on-stream due to catalyst deactivation.

The C_2H_4 formation rate, selectivity, and carbon deposition are shown as a function of residence time in Figure 6b. An increase of residence time leads to a significant decrease of the ethylene formation rate and increase of carbon deposition up to 0.31 s. For example, the formation rates of 0.6 Cr/BC were 1.57×10^{-6} and 2.2×10^{-7} mol/(m^2 s) for residence times of 0.06 and 0.31 s, respectively, and the amounts of carbon deposited 3.0×10^{-4} and 3.9×10^{-4} g/m^2. At residence times longer than 0.31 s, no significant further variation in the ethylene formation rate and carbon deposition was observed. C_2H_4 selectivity fell approximately linearly with increasing residence time from 100 to 94%, indicating that the methane formation rate also increases.

Ethane dehydrogenation was conducted with 0.2 g of Cr/BC and a residence time of 0.13 s; the ethylene formation rate is shown as an inverse function of temperature in Figure 7. It might seem that there is no difference in temperature dependence of the formation rate between residence times of 0.63 and 0.13 s, but a greater temperature dependence of C_2H_4

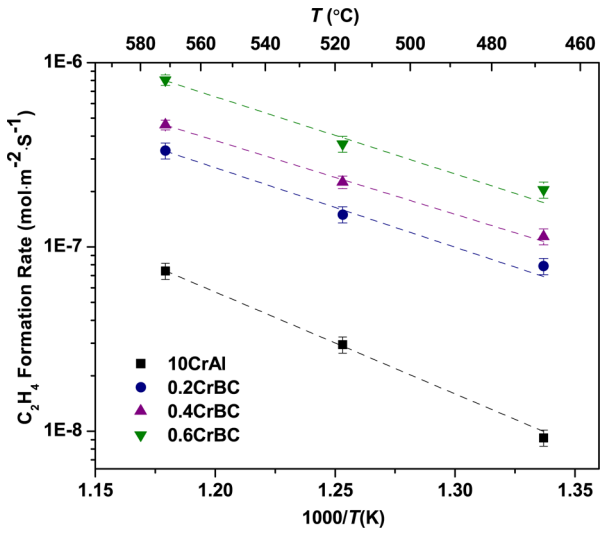

Figure 7. Arrhenius plot of ethylene formation rate over Cr/BC and 10 Cr/Al at a residence time of 0.13 s.

dx.doi.org/10.1021/cs501314w | ACS Catal. 2015, 5, 95−103

formation rate was observed at a residence time of 0.13 s. This supported Cr catalyst on BC was compared with 10 wt % Cr supported on γ-Al_2O_3 catalyst (10 Cr/Al), which was fabricated in same way as for Cr/BC: by the incipient wetness procedure.[10,28] The ethylene formation rates of 10 Cr/Al were 9.2×10^{-9}, 2.9×10^{-8}, and 7.4×10^{-8} mol/m^2·s at 475, 525, and 575 °C; these rates were about 1 order of magnitude lower than those for 0.6 Cr/BZ. The calculated apparent activation energy was 26.3 kcal/mol. This is in good agreement with a previous report,[8] where 27.5 kcal/mol was obtained in Cr/SiO_2.

3.4. Influence of H_2 Addition on Carbon Deposition. Various groups have sought to inhibit carbon deposition by addition of H_2, H_2/O_2, CO_2, or H_2O to the reactor feed.[8,36−39] Figure 8a shows the effect of H_2 addition to the feed at varying

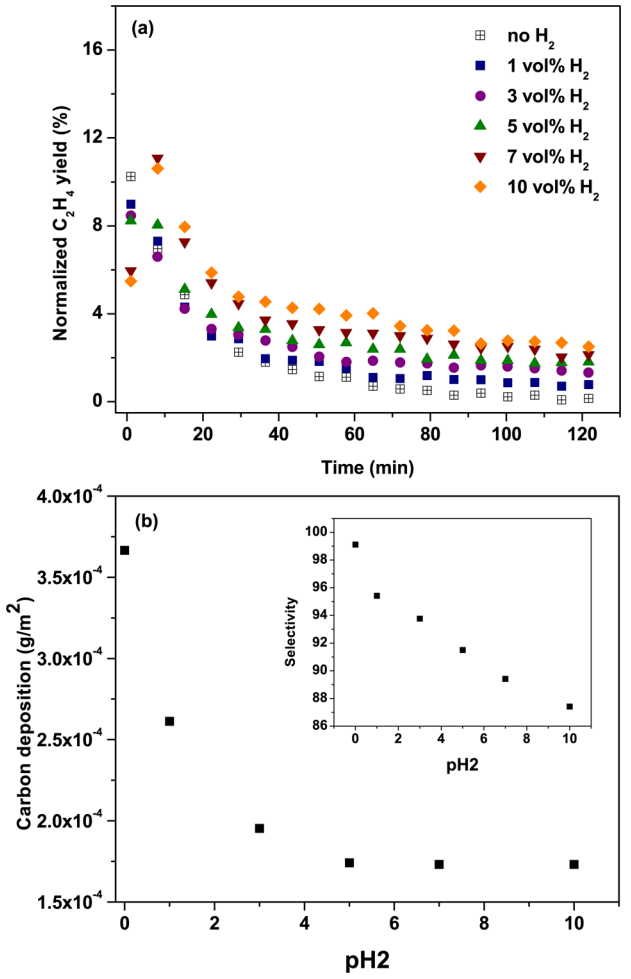

Figure 8. (a) Normalized ethylene yields versus time on-stream over 0.6 CrBC at 575 °C in the presence of H_2. (b) Amount of carbon deposition and selectivity to ethylene at 1 min on-stream (inserted figure) as a function of concentration of H_2.

H_2 contents ranging from 0 to 10 vol % for 0.2 g of 0.6 Cr/BC at 575 °C and a residence time of 0.13 s. In initial measurements at 1 min, an increase of H_2 partial pressure results in a decrease of ethylene yield: 15.9, 9.8, 8.5, 8.2, 6.0, and 5.5% for 0, 1, 3, 5, 7, and 10 vol % of H_2, respectively. In contrast, steady-state catalytic activity after 60 min shows quite a different trend; the yields at 120 min are 0.8, 0.8, 1.3, 1.8, 2.2, and 2.5%. Note that this is in contrast to the same deactivated rate for all catalysts in the absence of H_2 in the feed.

It should also be noted that, for H_2 addition above 5 vol %, there is a delay in the onset of deactivation, observable as a plateau or increase in yield as a function of time on-stream at short times. In addition, H_2 addition leads to a decrease in C_2H_4 selectivity: 99.1, 95.4, 93.7, 91.5, 89.4, and 87.4% for 0, 1, 3, 5, 7, and 10 vol % H_2 addition. TPO was conducted to investigate the amount of carbon deposited on Cr catalysts as a function of H_2 vol % (Figure 8b). Carbon deposition significantly decreases with increasing H_2 content until 5 vol % of H_2. The amounts of carbon deposited after ethane dehydrogenation for 2 h were 3.7, 2.6, 1.95, and 1.74×10^{-4} g/m^2 for 0, 1, 3, and 5 vol % of H_2. No further decrease of carbon deposition was observed above 5 vol % of H_2.

3.5. XPS Measurement. XPS measurements were performed to investigate the oxidation state of Cr in 0.2 Cr/BC, 0.2 Cr/BZ, and 10 Cr/Al (Figure 9). The sample

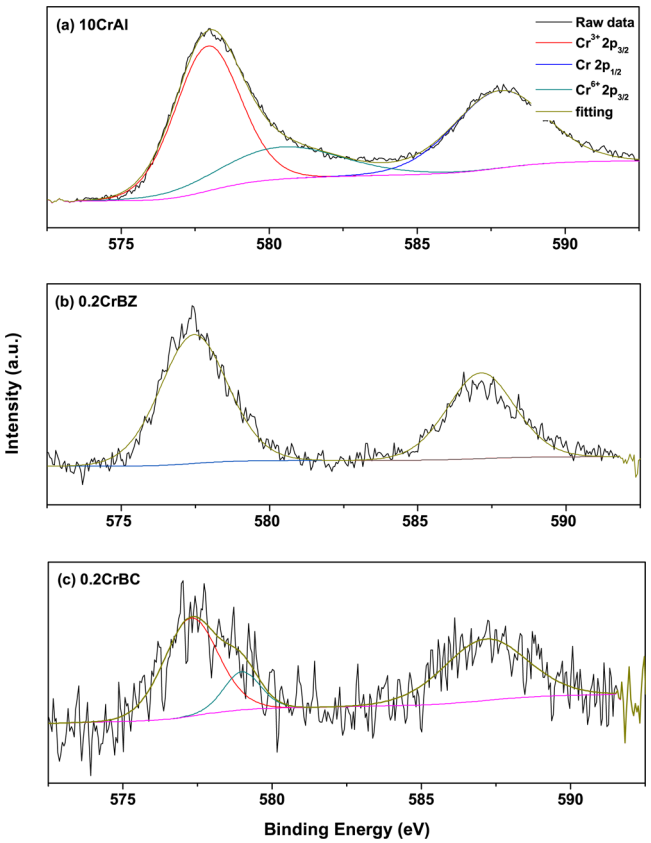

Figure 9. XPS spectra for (a) 10 Cr/Al, (b) 0.2 Cr/BZ, and (c) 0.2 Cr/BC.

pretreatment prior to XPS was the same as that prior to the catalytic function tests. All Cr 2p spectra were comprised of two main peaks with binding energies of ~577 and 586 eV, associated with Cr $2P_{3/2}$ and Cr $2P_{1/2}$ photoelectrons, respectively. As shown in Figure 9, Cr^{3+} Cr $2P_{3/2}$ overlaps with Cr^{6+} Cr $2P_{3/2}$ in the XPS spectra; thus, these were deconvoluted using the CasaXPS program by curve fitting with the mixed Gaussian−Lorentzian peaks. For 0.2 Cr/BZ, only one symmetric Cr $2P_{3/2}$ peak was observed at 577.5 eV, indicating the presence of only one chemical state, Cr^{3+}. In contrast, 10 Cr/Al and 0.2 Cr/BC show an additional peak characteristic of Cr^{6+} Cr $2P_{3/2}$ at binding energies of 580.4 and

dx.doi.org/10.1021/cs501314w | ACS Catal. 2015, 5, 95−103

578.9 eV, respectively. The presence of this peak is clear in the 10 Cr/Al sample and is observed as an asymmetry in the 0.2 Cr/BC peak at the expected position for the Cr^{6+} Cr $2P_{3/2}$.[21,40−42] The XPS-derived surface concentrations of atomic Cr and the ratios of different chromium oxidation states are summarized in Table 2. The ratio was calculated by measuring the area of characteristic peaks of deconvoluted Cr species. Due to the low signal-to-noise ratio for the XPS data on 0.2 Cr/BC, we also utilized an RGA to probe for Cr^{6+} by observing trace CO_2 production during the initial stages of the reaction over a fresh catalyst. While still not completely conclusive, the combination of these results strongly suggests that Cr^{6+} is present on the fresh 0.2 Cr/BC catalyst.

Table 2. XPS Data

	10 Cr/Al	0.2 Cr/BZ	0.2 Cr/BC
surface concn of Cr (atom %)	1.2	1.5	0.7
XPS (eV)			
Cr^{6+} $2p_{3/2}$	580.4		578.9
Cr $2p_{1/2}$	587.7	587.2	587.4
Cr^{3+} $2p_{3/2}$	577.9	577.5	577.3
Cr^{6+}/Cr^{3+}	0.47	0	0.26

4. DISCUSSION

Proton-conducting oxides, $BaZrO_3$ (BZ) and $BaCeO_3$ (BC), were tested as support materials for Cr catalysts for ethane dehydrogenation. As shown in Figure 1, it was demonstrated that a pure perovskite crystal structure was obtained; Cr was not observed in supported Cr catalyst (Cr/BZ and Cr/BC) due to the low amount of Cr loaded (0.2−0.6 wt %) (Figure 1b,d). No detrimental effect of the incipient wetness synthesis method on the crystal structure was observed below 5 wt % Cr loading, indicating the compatibility of BZ and BC with Cr catalyst.

Our results demonstrate the promise of proton-conducting ceramic supports for Cr catalysts in ethane dehydrogenation. In Figure 7, the BC-supported catalyst shows more than 1 order of magnitude higher C_2H_4 formation rate than the 10 wt % Cr/Al_2O_3 catalyst reported herein and the 0.5 wt % Cr on Al_2O_3 supported catalyst reported by Lugo et al.[8] While these catalysts have different total Cr contents, the Cr surface concentrations for both catalysts in this study were comparable: 0.19 and 0.11 g/m^2 for 10 Cr/Al and 0.2 Cr/BC, respectively. Furthermore, XPS-derived Cr atomic surface concentrations were 1.2 and 0.7 atom % for the same samples (Table 2). Note that all of the catalysts show high selectivity to ethylene, over 94% of the gas-phase product within all ranges of residence time utilized in this study, indicating that in all cases dehydrogenation of surface CH_3* is more rapid than hydrogenation to CH_4.

We then turn to possible reasons for this higher activity. Lugo et al.[8] suggested that similar catalytic activities between Cr/Al_2O_3 and Cr/SiO_2 indicate no significant electronic effect of these supports on the Cr active phase. In contrast, our results clearly show a significant influence of support on Cr in terms of C_2H_4 formation rate, selectivity, and carbon deposition. We propose that the observed higher activity of Cr/BZ in comparison with Cr/BC can be explained by the XPS data, where the existence of Cr^{6+} was observed only in Cr/BC. This is in agreement with the conclusion of Lugo et al. that more reduced Cr catalysts lead to higher catalytic activity in ethane dehydrogenation. Note that oxidized Cr/BZ showed significantly low ethane conversion to ethylene in comparison to the reduced species on initial measurement (Figure S1, Supporting Information). The conversion rapidly increased for the first 20 min and then decreased. This implies that the initial state of Cr prior to reduction in hydrogen was mostly Cr^{6+}, which over BZ was easily reduced to Cr^{3+} by hydrogen as a byproduct of ethane dehydrogenation or deposited carbon. Our XPS results also indicate that Cr might be reduced more easily on BZ than on BC.

Our initial hypothesis in this study was that the ability of a proton-conducting support to incorporate protons into the bulk may enhance the observed rates for ethane dehydrogenation. We have previously demonstrated that proton incorporation in these materials occurs via hydrogen dissociation on a metal, followed by spillover onto the oxide surface, with subsequent incorporation into the oxide.[10] We suggest that facile proton transport to and within the proton-conducting support materials plays a role in enhancing the observed rate, suggesting the possibility of a proton analogy to a Mars−van Krevelen mechanism. Our hypothesis could also be supported by the reports of Galvita et al.[9] showing that low concentrations of adsorbed hydrogen promoted ethane dehydrogenation by promoting the removal of hydrogen from surface ethyl groups, C_2H_5*. In our case, it could be that a mobile bulk proton may play a role similar to that of the adsorbed hydrogen; however, this hypothesis requires further investigation with different supports and a wider range of reactions and reaction conditions to be proven conclusively.

A significant difference between the two proton-conducting supports is the relatively gradual deactivation observed for Cr/BC in comparison with Cr/BZ (Figure 2). At the highest measurement temperature, the Cr/BC catalyst shows no deactivation until 40 min on-stream. In contrast, the Cr/BZ catalyst deactivates rapidly. One possibility is that the BC catalyst is more resistant to carbon deposition; however, our TPO results indicate that significantly more carbon was deposited on Cr/BC than on Cr/BZ, suggesting that this is not the case. A somewhat similar trend was observed by Olsbye et al.,[24] who studied ethane dehydrogenation over Cr/Al_2O_3 and found a maximum in ethylene yield after 10 min on-stream. One proposed theory is that large surface hydrocarbons are active for ethane dehydrogenation.[43] However, Olsbye et al.[24] conducted isotopic labeling experiments to demonstrate that this is not the case.

A delayed maximum in ethylene yield was also observed in propane dehydrogenation over Cr/Al_2O_3.[23] In the study, operando UV−vis spectra showed a decrease of the Cr^{6+} CT band with increasing time on-stream, with a simultaneous increase in the Cr^{3+} d−d transition band, implying reduction of CrO_3 to Cr_2O_3. We propose that the observed relative stability and sustained high ethylene yield observed for Cr/BC, especially at 575 °C, is related to the reduction of Cr reduction from Cr^{6+} to Cr^{3+}. This is supported by the XPS data for our samples showing the presence of Cr^{6+} only in Cr/BC; the Cr/BZ catalyst deactivates more rapidly and does not show any Cr^{6+}.

It is not clear if Cr^{6+} is reduced to Cr^{3+} by adsorbed hydrogen or deposited carbon, since hydrogen is also produced in ethane dehydrogenation. Nijhuis et al.[23] reported that a small amount of CO_2 was observed by mass spectrometry at the beginning of propane dehydrogenation, mentioning that the CO_2 is formed by the reduction of Cr^{6+} to Cr^{3+}. Any observation of water was not mentioned. In our experiment, simultaneous production of not only small (less than ∼0.1 vol

dx.doi.org/10.1021/cs501314w | ACS Catal. 2015, 5, 95−103

%) amounts of CO_2 but also H_2O was detected by mass spectrometry at short times on-stream. Thus, it is not clear whether the primary reducing agent is adsorbed hydrogen or carbon. Since our samples were reduced in hydrogen prior to reaction, it seems more likely that carbon is the reducing agent upon introducing ethane.

We then turn to the source of the carbon: by direct means from ethane or via the secondary reaction of product ethylene. Varying the reactor residence time for the Cr/BC catalyst facilitates insight into this process. As the residence time decreases, the amount of product ethylene increases, and the amount of carbon deposited decreases. This suggests that carbon formation is more likely from product ethylene than directly from ethane. Furthermore, Galvita et al.[9] reported that methane formation from product ethylene is more rapid than directly from ethane over platinum supported over calcined hydrotalcite in the presence of hydrogen, also supporting carbon formation from product ethylene. It should be noted that methane formation directly from ethane prevails in the absence of hydrogen. We carefully propose that hydrogenolysis of ethane might be prevented by proton in oxide, methane and carbon is formed from product ethylene. Therefore, we propose that a short contact time is required to optimize ethylene production through inhabitation of a secondary reaction of ethylene.[4]

Several researchers have investigated how to suppress carbon deposition; for example, addition of H_2O[4] and CO_2 were tried by Lugo et al.,[8] where water only leads to more rapid deactivation, with no effect of CO_2. Carbon formation rapidly deactivates these catalyst systems, requiring costly cyclic regeneration if this system were to be employed industrially; in our limited cycling the catalyst shows no degradation. Decreased carbon deposition was reported by Galvita et al.[9] upon addition of H_2 to the ethane feed. We examined the influence of H_2 addition on 0.2 g of 0.6 Cr/BC in concentrations ranging from 0 to 10 vol % in a 10% ethane/N_2 feed. Our results are in agreement with those in the literature.[9] Increasing the concentration of H_2 leads to decreases in initial ethylene yield and selectivity to ethylene, while steady-state activity increased. Galvita et al.[9] reported that an excess amount of adsorbed hydrogen plays a detrimental role for ethylene formation, since it increases the back-formation of ethane from C_2H_5* and hydrogenation of CH_3* to form methane. Our result also shows a decrease in the selectivity to ethylene with increasing H_2 contents to 87.4% at 10 vol % of H_2. Our experiment using cofed water into reactant has only a detrimental effect on ethane dehydrogenation; significantly lower ethylene production was observed. This is in good agreement with Lugo et al.[8] and our previous report.[10]

5. CONCLUSION

This study clearly demonstrates the potential of proton-conducting oxides as Cr catalyst supports for short contact time ethane dehydrogenation. At a residence time of 0.13 s, 0.6 Cr/BC showed more than 1 order of magnitude higher ethylene formation rate in comparison to those of 10 Cr/Al in our study and 0.5% Cr/Al in the literature. XPS measurement indicated that Cr^{3+} is the most active oxidation state for ethane dehydrogenation and that this oxidation state is more prevalent on a barium zirconate support in comparison to barium cerate. A significant decrease in ethylene yield and selectivity to ethylene and increasing carbon deposition with increasing residence time indicate that product ethylene can be consumed by secondary reactions to form carbonaceous deposits. Addition of H_2 into the reactant feed resulted in resistance to carbon deposition at the expense of a slight decrease in conversion and selectivity to ethylene. While all of the samples showed deactivation due to coke, the use of the higher activity barium cerate or barium zirconate support materials could enable commercial productivity to be maintained at reduced operating temperatures with associated reduced carbon deposition rates.

■ ASSOCIATED CONTENT

Supporting Information

The following file is available free of charge on the ACS Publications website at DOI: 10.1021/cs501314w.

Normalized ethane conversion to ethylene versus time on stream over reduced 0.6Cr/BZ and oxidized 0.6Cr/BZ (PDF)

■ AUTHOR INFORMATION

Corresponding Author

*S.M.: e-mail, mcintosh@lehigh.edu; tel, +1-610-758-6835; fax, +1-610-758-5057.

Notes

The authors declare no competing financial interest.

■ ACKNOWLEDGMENTS

This work was partially funded by the National Science Foundation under grant 1101817.

■ REFERENCES

(1) Bhasin, M. M.; McCain, J. H.; Vora, B. V.; Imai, T.; Pujadó, P. R. *Appl. Catal. A: Gen.* **2001**, *221*, 397−419.
(2) Shen, W.; Wang, Y.; Shi, X.; Shah, N.; Huggins, F.; Bollineni, S.; Seehra, M.; Huffman, G. *Energy Fuels* **2007**, *21*, 3520−3529.
(3) Shah, N.; Wang, Y.; Panjala, D.; Huffman, G. P. *Energy Fuels* **2004**, *18*, 727−735.
(4) Huff, M.; Schmidt, L. D. *J. Phys. Chem.* **1993**, *97*, 11815−11822.
(5) Bañares, M. A. *Catal. Today* **1999**, *51*, 319−348.
(6) Weckhuysen, B. M.; Wachs, I. E.; Schoonheydt, R. A. *Chem. Rev.* **1996**, *96*, 3327−3350.
(7) Weckhuysen, B. M.; Schoonheydt, R. A. *Catal. Today* **1999**, *51*, 223−232.
(8) Lugo, H. J.; Lunsford, J. H. *J. Catal.* **1985**, *91*, 155−166.
(9) Galvita, V.; Siddiqi, G.; Sun, P.; Bell, A. T. *J. Catal.* **2010**, *271*, 209−219.
(10) Shin, H. H.; McIntosh, S. *J. Mater. Chem. A* **2013**, *1*, 7639.
(11) Shin, H. H.; McIntosh, S. *ECS Electrochem. Lett.* **2013**, *2*, F88−F91.
(12) Vernoux, P.; Lizarraga, L.; Tsampas, M. N.; Sapountzi, F. M.; Lucas-Consuegra, A. D.; Valverde, J.; Souentie, S.; Vayenas, C. G.; Tsiplakides, D.; Balomenou, S.; Baranova, E. A. *Chem. Rev.* **2013**, *113*, 8192−8260.
(13) Fu, X.; Luo, J.; Sanger, A. R.; Danilovic, N.; Chuang, K. T. *Chem. Commun.* **2010**, *46*, 2052−2054.
(14) Fu, X.; Luo, X.; Luo, J.; Chuang, K. T.; Sanger, A. R.; Krzywicki, A. *J. Power Sources* **2011**, *196*, 1036−1041.
(15) McIntosh, S.; Gorte, R. J. *Chem. Rev.* **2004**, *104*, 4845−4865.
(16) Kim, D. H.; Park, J. L.; Park, E. J.; Kim, Y. D.; Uhm, S. *ACS Catal.* **2014**, *2014*, 3117−3122.
(17) Zhong, J.; Li, H.; Zhong, L.; Xiao, P.; Xu, X.; Yang, X.; Zhao, Z.; Li, J. *ACS Catal.* **2014**, *4*, 2917−2940.
(18) van den Bossche, M.; McIntosh, S. *J. Catal.* **2008**, *255*, 313−323.
(19) Azimova, M. A.; McIntosh, S. *J. Electrochem. Soc.* **2011**, *158*, B1532−B1538.

(20) Lillehaug, S.; Børve, K. J.; Sierka, M.; Sauer, J. *J. Phys. Org. Chem.* **2004**, *17*, 990−1006.
(21) Cavani, F.; Koutyrev, M.; Trifirò, F.; Bartolini, A.; Ghisletti, D.; Iezzi, R.; Santucci, A.; Del Piero, G. *J. Catal.* **1996**, *158*, 236−250.
(22) De Rossi, S.; Ferraris, G.; Fremiotti, S.; Indovina, V.; Cimino, A. *Appl. Catal. A: Gen.* **1993**, *106*, 125−141.
(23) Nijhuis, T. A.; Tinnemans, S. J.; Visser, T.; Weckhuysen, B. M. *Phys. Chem. Chem. Phys.* **2003**, *5*, 4361−4365.
(24) Olsbyea, U.; Virnovskaiaa, A.; Prytza, Ø.; Tinnemansb, S. J.; Weckhuysen, B. M. *Catal. Lett.* **2005**, *103*, 143−148.
(25) Norby, T. *Solid State Ionics* **1999**, *125*, 1−11.
(26) H. E. van Doorn, R.; Kruidhof, H.; Nijmeijer, A.; Winnubst, L.; J. Burggraaf, A. *J. Mater. Chem.* **1998**, *8*, 2109−2112.
(27) Vogel, A.*Textbook of Quantitative Inorganic Analysis*; Longman Scientific and Technical: Harlow, United Kingdom, 1986.
(28) Levy, P.; Primet, M. *Appl. Catal.* **1991**, *70*, 263−276.
(29) Knight, K. S.; Bonanosb, N. *J. Mater. Chem.* **1994**, *4*, 899−901.
(30) Knight, K. S. *Solid State Ionics* **2001**, *145*, 275−294.
(31) Takeuchi, K.; Loong, C. K.; Richardson, J. W., Jr.; Guan, J.; Dorris, S. E.; Balachandran, U. *Solid State Ionics* **2000**, *138*, 63−77.
(32) Glöckner, R.; Islam, M. S.; Norby, T. *Solid State Ionics* **1999**, *122*, 145−156.
(33) Stokes, S. J.; Islam, M. S. *J. Mater. Chem.* **2010**, *20*, 6258−6264.
(34) Braun, A.; Duval, S.; Ried, P.; Embs, J.; Juranyi, F.; Strässle, T.; Stimming, U.; Hempelmann, R.; Holtappels, P.; Graule, T. *J. Appl. Electrochem.* **2009**, *39*, 471−475.
(35) Duval, S. B. C.; Holtappels, P.; Vogt, U. F.; Stimming, U.; Graule, T. *Fuel Cells* **2009**, *9*, 613−621.
(36) Virnovskaia, A.; Rytter, E.; Olsbye, U. *Ind. Eng. Chem. Res.* **2008**, *47*, 7167−7177.
(37) Yu, C.; Ge, Q.; Xu, H.; Li, W. *Ind. Eng. Chem. Res.* **2007**, *46*, 8722−8728.
(38) Tasbihi, M.; Feyzi, F.; Amlashi, M. A.; Abdullah, A. Z.; Mohamed, A. R. *Fuel Process. Technol.* **2007**, *88*, 883−889.
(39) Kogan, S. B.; Schramm, H.; Herskowitz, M. *Appl. Catal. A: Gen.* **2001**, *208*, 185−191.
(40) Rao, T. V. M; Yang, Y.; Sayari, A. *J. Mol. Catal. A: Chem.* **2009**, *301*, 152−158.
(41) Rao, T. V. M; Zahidi, E. M.; Sayari, A. *J. Mol. Catal. A: Chem.* **2009**, *301*, 159−165.
(42) Xing, T.; Wan, H.; Shao, Y.; Han, Y.; Xu, Z.; Zheng, S. *Appl. Catal. A: Gen.* **2013**, *468*, 269−275.
(43) Mestl, G.; Maksimova, N. I.; Keller, N.; Roddatis, V. V.; Schlögl, R. *Angew. Chem., Int. Ed.* **2001**, *40*, 2066−2068.